Biomaterials Science

Accepted Manuscript

ROYAL SOCIETY OF CHEMISTRY

rsc.li/biomaterials-science

View Article Online
DOI: 10.1039/D5BM01812A

Engineering immunostimulatory nanocarriers: TLR7-agonist conjugated poly(beta-amino ester) mRNA delivery systems

Hulya Bayraktutan[abc], Amr Elsherbeny[ab], Rafał J. Kopiasz[ad], Charlotte Galley[e], Nurcan Gumus[abfg], Clare L Bennett[e], Cameron Alexander*[a] and Pratik Gurnani*[h]

[a] Division of Molecular Therapeutics and Formulation, Boots Science Building, School of Pharmacy, University of Nottingham, Nottingham, NG7 2RD, UK

[b] Biodiscovery Institute, School of Medicine, University of Nottingham, Nottingham, NG7 2UH, UK.

[c] Department of Pharmaceutical Biotechnology, Faculty of Pharmacy, Hacettepe University, Ankara 06100, Türkiye

[d] Warsaw University of Technology, Faculty of Chemistry, Noakowskiego 3 St., 00-664, Warsaw, Poland

[e] Department of Haematology, UCL Cancer Institute, 72 Huntley Street, University College London, London, WC1E 6DD, UK

[f] Department of Medical Biology, Faculty of Medicine, Izmir Bakircay University, Izmir, Türkiye

[g] Department of Medical Pharmacology, Faculty of Medicine, Izmir Bakircay University, Izmir, Türkiye

[h] UCL School of Pharmacy, University College London, 29-39 Brunswick Square, Bloomsbury, London, WC1N 1AX, UK

Abstract

Messenger RNA (mRNA) technology serves as a powerful foundation for novel vaccines and treatments. Ensuring effective delivery of RNA medicines requires vectors due to the poor cellular association of naked mRNA and susceptibility to degradation by endogenous nucleases. Recently, nanoparticle-based carries have attracted significant attention, particularly poly(beta-amino esters) (PBAEs) which have showed promise as mRNA delivery systems. The first generation of nanoparticle-encapsulated mRNA vaccines have been highly successful in protecting against severe COVID-19 disease, but the durability of immune response remains short and hence there is a need for delivery systems which enhance the robustness of immune response. In this study, we report the development of a TLR7-adjuvanting PBAE through direct conjugation of Loxoribine, a potent TLR7 agonist. We observed that the Loxoribine conjugated PBAE was able to condense self-amplifying RNA (saRNA) efficiently into small (100 - 200 nm) polyelectrolyte nanoparticles with complete incorporation of the nucleic acid. Formulations specifically at w/w ratio 128 showed high transfection in HEK293T and DC2.4 cell lines with good cytotoxicity profiles. In addition, TLR activation assays using TLR7 reporter HEK-Blue cells showed that Loxoribine conjugated formulations can efficiently agonise TLR7 with some synergy observed between Loxoribine and the delivered saRNA. Although potent activation was observed in model cell lines, evaluation in primary bone marrow derived dendritic cells showed minimal upregulation of CD86 an established activation marker and less than 2% transfection efficiency. Consequently, these findings suggest the potential of adjuvanted PBAE nanoparticles for enhanced RNA vaccines however further development is needed to improve activity in primary immune cells.

Key words: saRNA, PBAE, Loxoribine, TLR7 agonist, polyplex, HEK293T, DC2.4 and HEK-BLUE cells

View Article Online
DOI: 10.1039/D5BM01812A

Introduction

Messenger RNA technology represents a safe, potent and manufacture-friendly route to express transiently endogenous or engineered proteins in a target cell or tissue. mRNA has therefore been widely studied for the development of novel vaccines against infectious disease and immunotherapies for a variety of malignancies [1, 2]. These operate by administering mRNA encoding for pathogen or malignant cell surface protein epitopes to train the immune system to recognise these and eliminate them either on infection by the pathogen, or as against cancer tumours/cells expressing those epitopes [3, 4]. In both applications, the quality and robustness of the immune response is critical in the eventual adaptive immune response against the target antigen and therefore therapeutic/prophylactic performance.

Naked mRNA displays poor cellular association and susceptibility to degradation from endogenous nucleases, meaning that a suitable delivery vector is required to protect the nucleic acid cargo and facilitate its transportation to its target in the cytosol [5, 6]. These delivery systems are typically nanoparticle-based materials, such as lipid nanoparticles (LNP), which have been clinically used for three approved nucleic acid products (Onpattro, Spikevax and Comirnaty) [7]. However, their chemical versatility and limited intellectual property space creates an urgent need for alternative delivery systems. Among these, polycations are now recognised as a potent but clinically immature delivery approach [8, 9]. These operate by condensing negatively charged mRNA into small (50-200 nm) polyplex nanoparticles with positively charged cationic polymers through opposing electrostatic interactions [10, 11]. One promising subclass is poly(beta-amino ester)s (PBAEs), which contain hydrolysable ester bonds in their backbone, enabling biodegradability and facilitating RNA release [12-14]. Their highly tunable chemistry supports adaptation for different nucleic acid cargos, making them strong candidates for RNA delivery [15-17]. In addition to their delivery capacity, certain PBAEs can influence immune responses, providing a platform that can be further tailored with immunostimulatory components [18]. The significantly broader chemical versatility of these materials makes these ideal systems for improving the immune response of mRNA vaccines.

In principle, messenger RNA vaccines and immunotherapies display self-adjuvanting behaviour, due to the agonist properties of exogenous RNA on endosomal (Toll-like receptor 7/8) and cytosolic (RIG-I, MDA-5) single stranded RNA sensors which mimic the inflammatory process of an infective RNA virus [19, 20]. However, the condensation of mRNA into nanoparticles and use of modified nucleotides, such as 1-methylpseudouridine (m1ψ) hinders the activation of these processes in antigen-presenting cells (APCs) which weakens the initial steps of the adaptive immune response [21]. However, excessive activation of these inflammatory processes simultaneously puts APCs into an ‘anti-proliferative’ state, thus shutting down the cells’ protein synthesis machinery, and reducing the translation efficiency of the delivered mRNA construct [21, 22].

Traditional vaccines and immunotherapies achieve a robust immune response by utilising adjuvants, immunostimulatory molecules which are co-formulated with the active ingredient [23]. Adjuvanticity can be introduced either from a humoral immunity perspective, through controlled release of the antigen, or preferably direct activation of cellular immunity through the co-formulation of molecules which simulates the natural infection process by binding to pathogen recognition receptors (PRRs) at the immune cell surface [24]. Key example of these are agonists for Toll-like receptors (TLRs), a specific PRR class found in APCs, macrophages and other cells which, when stimulated, elicit downstream expression of pro-inflammatory cytokines which form the innate immune response [25].

Development of adjuvanted mRNA formulations, which co-deliver the antigen encoding nucleic acid and adjuvant to the same cells could therefore represent a powerful strategy to strengthen and broaden the immune response of mRNA vaccines, whilst providing a flexible platform to mitigate any inflammatory induced inhibition of mRNA translation [26, 27]. There is significant evidence that LNP formulations display intrinsic adjuvanticity, but these effects are not always predictable and are dependent on the cationic/ionisable lipid structures [28, 29]. In contrast, there has been significant progress in targeted adjuvant formulations for mRNA vaccines and therapies, often through co-formulation or conjugation of TLRa’s, such as polyinosine-cytosine (polyI:C, TLR3a), imidazoquinolines (TLR7/8a) and CG rich oligonucleotides (CpG-ODN, TLR9a) from an LNP perspective [30-32]. Meanwhile the few limited reports of adjuvanted polycation delivery systems focus on co-formulation of

View Article Online
DOI: 10.1039/D5BM01812A

polyI:C and CpG-ODNs, however direct conjugation of a TLR agonist adjuvant has not been reported for polymer-based mRNA formulations to our knowledge [33, 34].

Herein, we report the development of a TLR7a conjugated polycation as a potential adjuvanted formulation for mRNA and self-amplifying mRNA, an mRNA technology which includes replicase genes, amplifying the construct within the cytosol. saRNAs can therefore enhance protein expression levels at significantly lower doses, lengthening expression half-life and reducing the cost compared to mRNA [35, 36]. We utilised the intrinsic chemistry of Loxoribine (a guanosine analogue known as a TLR7 agonist) to conjugate this on the end-groups of a PBAE cationic polymer, which are now well-established polymeric delivery systems for mRNA and saRNA modalities. The Loxoribine-PBAE conjugate was then formulated with saRNA to form adjuvanted polyplexes, which were characterised for their delivery efficiency, transfectability and ability to stimulate the TLR7 pathway in cells. Finally, the polyplexes were further evaluated in bone marrow dendritic cell (BMDC) experiments to assess dendritic cell activation.

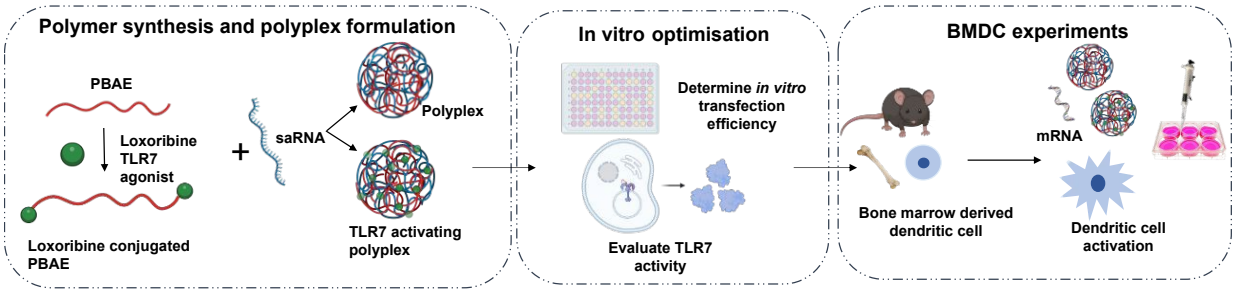

Figure 1. Schematic representation of PBAE synthesis, polyplex assembly, analysis of in vitro transfection and toxicity profiles, the evaluation of TLR7 activation and bone marrow dendritic cell (BMDC) experiments to assess dendritic cell activation.

Materials and Methods

Materials

1,4-Butanediol diacrylate (BDD), 5-aminopentan-1-ol (5-AP), 2,2'-(ethylenedioxy)bis(ethylamine), 3-mercaptopropanyl-N-hydroxysuccinimide ester, tris(2-carboxyethyl)phosphine (THP), triethylamine (TEA), fluorescein isothiocyanate (FITC), diethyl ether, tetrahydrofuran, sodium acetate (NaOAc) buffer (pH:5.0) and the dye Gel Red were purchased from Sigma-Aldrich. Loxoribine was purchased from InvivoGen. Dichloromethane (DCM), *N*,*N*-dimethylformamide (DMF), acetonitrile (ACN), tetrahydrofuran (THF), hexane, diethyl ether, dimethyl sulfoxide (DMSO), loading buffer, Tris-acetate-EDTA (TAE) buffer, tris-(2-hydroxyethyl) phosphine (THP), Lipofectamine Messenger MAX™, Hoechst 33342, Lysotracker red and 96-well plates were obtained from ThermoFisher. Dulbecco's Modified Eagle Medium (DMEM) cell culture medium, RPMI 1640 cell culture medium, HEK-Blue Detection medium, fetal bovine serum (FBS) and Opti-MEM were bought from Gibco, Invitrogen, Carlsbad, CA, USA. PrestoBlue reagent and ONE-Glo D-luciferin substrate were purchased from Promega, UK. Self-amplifying RNA was synthesised as previously described [35]. mRNA was purchased from Trilink biotechnologies.

Instrumentation and Analysis

NMR Spectroscopy

All ^{1}H-NMR spectra were recorded in ppm (δ) at 400 MHz in d6-DMSO using a Bruker Advance III MHz spectrometer that was maintained at 25°C. To analyse the spectra MestReNova 6.0.2 copyright 2009 (Mestrelab Research S.L.) was applied.

View Article Online
DOI: 10.1039/D5BM01812A

Gel permeation Chromatography

The gel permeation chromatography (GPC) analysis was performed using the PL-50 instrument equipped with a dual angle light scatter (LS), viscometry (VS) and differential refractive index (DRI). The system was equipped with a PLgel 5 µm guard column and a 2 × PLgel Mixed D columns (300 × 7.5 mm). Dimethylformamide (DMF) with LiBr (0.1% wt/wt) was utilised as an eluent with a flow rate of 1 mL/min at 50°C. The instrument was calibrated with Poly(methyl methacrylate) standards (Agilent EasyVials) between 955500–550 g mol^{-1}. Using conventional calibration, Cirrus GPC software, dispersity (*Đ*) values, molecular weight (M_w) and experimental molar mass (M_n, SEC) were detected.

DLS and Zeta Potential

A Zetasizer nano-ZS90 (Malvern, Inc.) dynamic light scattering (DLS), instrument was used to characterise the particles in terms of their size, polydispersity index (PDI) and zeta potential. The instrument was used at 25°C to determine the zeta potential, average hydrodynamic diameters, and PDI of polyelectrolyte complexes.

Transmission Electron Microscopy

Briefly, glow discharged Formvar/carbon coated TEM grids were used, on which were placed the formulation samples (13 µL), which were left for 15 minutes, then the excess solution was removed and the samples allowed to dry at room temperature. Following this, 10 µL of 2% aqueous uranyl acetate was applied to each grid and left for 10 seconds. After air drying, imaging was performed using a Tecnai G2 Spirit TEM with BioTwin lens configuration (Thermo Fisher Scientific, Eindhoven, The Netherlands) at an accelerating voltage of 100kV.

Polymer Synthesis and Characterisation

pBDD-5AP

To BDD (1000 mg, 5 mmol) in DMSO (0.95 mL), 5-AP (470 mg, 4.56 mmol) in DMSO (2 mL) was added and the reaction was stirred at 90°C overnight. Then, the mixture was diluted with THF (2.94 mL), the product was isolated by precipitation from diethyl ether (40 mL), and further purified by re-dissolving in THF (3 mL) and precipitation in diethyl ether (40 mL) thrice. The product was dried under vacuum overnight yielding 1250 mg (85%) of a yellowish oil. Molecular weight determined by SEC: M_n = 6.2 kDa, M_w = 8.0 kDa, *Đ* = 1.3; for ^{1}H NMR see Spectrum S1 in Supplementary Information.

H_2N-(pBDD-5AP)-NH_2

To produce amine end-capped PBAEs, an excess amount of 2,2'-(ethylenedioxy)bis(ethylamine) (300 mg, 2.02 mmol) was added to the BDD-5AP (1000 mg) in DMSO (10 mL) in a 20 mL vial and the mixture was stirred for 24 hours at room temperature. Polymers were isolated by diluting the reaction mixture into THF (10 mL) followed by dropwise precipitation in diethyl ether (40 mL) thrice. The polymer was collected via centrifugation and dried under reduced pressure at 37°C and a yellow viscous liquid was obtained. Finally, polymers were stored at -20°C as 100 mg/mL solution in DMSO. Molecular weight determined by SEC: M_n = 6.6 kDa, M_w = 9.1 kDa, *Đ* = 1.4; for ^{1}H NMR see Spectrum S2 in Supplementary Information.

SH-(pBDD-5AP)-SH

To produce SH-end-capped PBAEs, an excess amount of mercaptopropanyl-N-hydroxysuccinimide ester (84.5 mg, 0.42 mmol) was added to H_2N-(pBDD-5AP)-NH_2 (500 mg) in DMSO (5 mL) in a 20 mL vial, lastly TEA (16.8 mg, 0.16 mmol) and THP (2.5 mg, 20 µmol) were added the mixture. The mixture was stirred for 3 hours at room temperature under Argon and UV conditions to avoid polymer crosslinking. Polymers were isolated by diluting the reaction mixture into THF (5 mL) followed by dropwise precipitation in diethyl ether (40 mL) thrice. The polymer was collected via centrifugation and dried under reduced pressure at 37°C and a yellow viscous liquid was obtained. Finally, polymers were stored at -20°C as 100 mg/mL solution in DMSO. Molecular weight determined by SEC: M_n = 6.9 kDa, M_w = 9.9 kDa, *Đ* = 1.4; for ^{1}H NMR see Spectrum S3 in Supplementary Information.

LOX-(pBDD-5AP)-LOX

Finally, to obtain LOX-end-capped PBAEs, an excess amount of Loxoribine (141 mg, 0.41 mmol) was added to HS-(pBDD-5AP)-SH (500 mg) in DMSO (5 mL) in a 20 mL vial, lastly TEA (16.8 mg, 166 µmol) and THP (2.5 mg) were added the mixture. The mixture was stirred for 3 hours at room temperature under argon and UV conditions to avoid polymer crosslinking. Then, the mixture was dialysed

View Article Online
DOI: 10.1039/D5BM01812A

(molecular weight cut-off 3.5 kDa) against DMSO (1 L) for 24 hours and DMSO solution was changed once. Afterwards, the mixture was precipitated in diethyl ether (40 mL) and to remove remaining DMSO re-dissolved in THF (5 mL) and was precipitated in diethyl ether (40 mL) thrice. The product was dried under vacuum overnight and obtained a dark yellowish viscous liquid. Molecular weight determined by SEC: M_n = 7.8 kDa, M_w = 11 kDa, $Đ$ = 1.4; for ^{1}H NMR see Spectrum S4 in Supplementary Information.

Synthesis of Fluorescently Labelled Polymers

LOX-(pBDD-5AP)-LOX polymer was dissolved in 5 mL DMSO (0.5 mg/ml) in a 20 mL vial. FITC was added to vials at a 1:10 (moles of end amine: FITC) molar ratio and TEA was added to mixture as 0.1 molar ratio. The reaction mixture was allowed to stir for 24 hours in the dark at room temperature. The reaction mixture was then dialysed in the dark using molecular weight cut-off 3,5 kDa against 250 mL NaOAc buffer (pH:5.0). Purification was continued for 4 days and the dialysis medium refreshed 2 times in a day. After freeze drying, FITC-labelled polymers were collected as a yellow solid and were stored at -20°C as 100 mg/mL solution in DMSO.

Polymer Buffering Capacity Assay

The buffering capacity of the polymers was evaluated by acid-base titration over the pH range of 10.0–3.0. Briefly, 2 mg of polymer was dissolved in 30 mL of 0.1 M NaCl aqueous solution, and the solution was adjusted to pH 10.0 using 0.1 M NaOH. Then, precise volumes (between 20-40 µL) 0.1 M HCl were added until a pH of 3 was achieved. The pH after each addition of HCl was recorded. 0.1 M NaCl was set as negative control.

Preparation of Polyplexes

Polyplexes were prepared by electrostatic interactions between positively charged polymers and negatively charged saRNA or mRNA by mixing various w/w ratios (32, 64 and 128). Firstly, the working dilutions of polymers and saRNA or mRNA were prepared in 25mM NaOAc buffer (pH:5.0). Depending on the desired w/w ratio, differing amounts of polymer stock solutions (100 mg/mL in DMSO) were mixed with nucleic acids in the buffer, gently mixed using a pipette and incubated at room temperature for 30 minutes. Whilst preparing the PBAE/saRNA complexes, taking a w/w 64 ratio as an example, 10 µg/mL of the RNA stock solution was mixed with 2.560 mg/mL PBAE by pipette using a 25mM NaOAc buffer.

Encapsulation Efficiency Using Ribogreen Assay

A fluorescence-based Quant-iT RiboGreen assay (ThermoFisher, UK) was utilised to be able to detect free RNA in solution after polymer encapsulation. Samples were diluted in 1× TE buffer (v/v 1:1) and the assay was performed according to the manufacturer's protocol. Samples were then loaded on a black, 96-well plate, and analysed for fluorescence on a microplate reader at an excitation of 485 nm and emission at 528 nm.

Determination of Drug Loading

The evaluation of Loxoribine amount in LOX-(pBDD-5AP)-LOX nanoparticles was conducted through high-performance liquid chromatography (HPLC) quantification. Initially, 1 mg of the LOX-end-capped formulation was suspended in 1 mL of 1M HCl and subjected to a 4-hour incubation at 37°C to facilitate nanoparticle degradation and release of the therapeutic agent. Subsequently, the drug content was analysed using a Shimadzu UFLC system (Shimadzu Corporation, Kyoto, Japan) equipped with a Hichrom 5 C18 column (250 × 4.6 mm) at room temperature. The mobile phase, composed of water and acetonitrile in a 20:80 ratio, flowed at 1 mL/min. A 20 µL injection volume was used, and the drug was monitored at 254 nm. Loxoribine exhibited a retention time of 2 minutes. The method demonstrated linear responses within the concentration range of 0.6-200 µg/ml. The results are presented as mean values ± standard deviation (SD). The drug loading was calculated using the following equation:

$$Drug\ load\ (\%) = \frac{weight\ of\ drug(mg)}{weight\ of\ formulation\ (mg)}\ x\ 100$$

View Article Online
DOI: 10.1039/D5BM01812A

Determination of Drug Loading Using Ultraviolet–visible

To assess the drug loading efficiency of the polymer formulations, UV-Vis spectroscopy was employed. Polymers were dissolved in 25 mM sodium acetate (NaOAc) buffer (pH 5.0) at a concentration of 1 mg/mL, ensuring complete solubilization. Serial dilutions of Loxoribine (ranging from 3 to 100 µg/mL) were also prepared using the same buffer to generate a standard calibration curve.

All solutions were transferred into quartz cuvettes and subjected to UV-Vis spectral analysis using a Tecan Spark spectrophotometer. Absorbance measurements were recorded at λmax = 251 nm and 300 nm, which correspond to the characteristic absorption peaks of Loxoribine. The drug loading was determined by comparing the absorbance values of polymer-loaded drug solutions to the standard calibration curve.

In vitro experiments

Cell Culture

Human embryonic kidney 293T (HEK293T) cells were a gift from Imperial College London and cultured in 10 % (v/v) FBS containing high glucose DMEM cell culture medium. DC2.4 cells were obtained from ATCC and cultured in RPMI 1640 cell culture medium. Media containing L-glutamine was supplemented with 4-(2-hydroxyethyl)-1-piperazineethanesulfonic acid (10mM), non-essential amino acids (0.1mM) and 10 % FBS. Human TLR7 transfected HEK cells (HEK-Blue™) cells were purchased from InvivoGen and cultured in 10 % (v/v) FBS containing high glucose DMEM cell culture medium. Absence of mycoplasma was confirmed using polymerase chain reaction. Cells were grown to 90 % confluence in a humidified incubator at 37°C (5% CO2) and detached with 1x trypsin/EDTA. Viability was assessed using Trypan Blue staining.

Cell Viability Assays

To investigate the cytotoxicity of the formulations, a cell viability assay was performed in the HEK293T, DC2.4 and HEK-BLUE cell lines. 24 hours prior to treatment, cells were seeded in a clear 96-well plate at a density of $20x10^3$ cells/well. For the treatment, the medium was aspirated, and cells were treated with 200 µL of Opti-MEM containing various w/w ratios of formulations complexed with 10 µg/ml fluc saRNA concentration (20 µL of polyplex solution). After 4 hours, nanoparticles were aspirated and 100 µL of complete medium was added to wells. At 24 hours posttreatment, each well was treated with 100 µL of 10 % PrestoBlue reagent and allowed to incubate for 1 hour. Then, the total volume was transferred to a black 96-well plate and the FLUOstar Omega plate reader (BMG LABTECH, UK) was used to determine the fluorescent intensity (540 nm – 590 nm) of each well and normalized to the medium control.

In Vitro Transfection Experiments

In vitro transfection experiments were performed in HEK293T and DC2.4 cell lines, and the commercially available transfection reagent Lipofectamine Messenger MAX™ was used as positive control. 24 hours prior to treatment, cells were seeded in a clear 96-well plate at a density of $20x10^3$ cells per well. For the treatment, the medium was aspirated, then cells were transfected with 200 µL of Opti-MEM containing various w/w ratios of formulations complexed with 10 µg/mL fluc saRNA concentrations (20 µL of polyplex solution). After 4 hours, nanoparticles were aspirated and 100 µL of medium was added to wells. At 24 hours post-treatment, 50 µL of media was removed then 50 µL of the ONE-Glo D-luciferin substrate was placed into each well and mixed well by pipette. Finally, the total 100 µL was placed in a 96-well plate and FLUOstar Omega plate reader (BMG LABTECH, UK) was used to determine the luminescence.

TLR7 Activation Assay

TLR7 activation was tested on human TLR7 transfected HEK cells (HEK-BLUE). The commercially available transfection reagent Lipofectamine Messenger MAX™ was used as positive control. 24 hours prior to treatment, cells were seeded in a clear 96-well plate at a density of $20x10^3$ cells per well. For the treatment, the medium was aspirated, then cells were transfected with 200 µL of HEK-Blue Detection medium containing polymers only (without saRNA, 20 µL) with different w/w ratios and various w/w ratios of formulations complexed with 10 µg/mL fluc saRNA concentrations (20 µL of polyplex

View Article Online
DOI: 10.1039/D5BM01812A

solution). At 24 hours post-treatment, absorbance was measured at 620 nm using a FLUOstar Omega plate reader (BMG LABTECH, UK).

Cellular Uptake of saRNA using Confocal Microscopy

HEK293T and DC2.4 cells were seeded in CellView™ 35 mm diameter glass bottom cell culture dishes at a density of 30 x 10^4 cells per well. For the treatment, the medium was aspirated, and cells were transfected with Opti-MEM containing FITC labelled LOX-end-capped formulation (LOX-(pBDD-5AP)-LOX) w/w 128 at 0.01 mg/mL. Cells were incubated for 2 hours at 37°C with 5% CO2. Then, nanoparticles were aspirated, and cells washed 3 times with PBS and stained with 10 µg/mL Hoechst 33342 and 75nM Lysotracker red applied in PBS solution. After 30 minutes, solution was aspirated, and cells were washed 3 times with PBS then FluoroBrite DMEM was added to cells. Imaging was performed using Leica confocal microscopy with LAS X software on DAPI, FITC and Lysotracker filters. ImageJ software was used to process the pictures.

Imaging Flow Cytometry

DC2.4 cells were seeded in a clear 6-well plate at a density of 40 x 10^5 cells per well. For the treatment, the medium was aspirated, and cells were transfected with Opti-MEM containing LOX-(pBDD-5AP)-LOX w/w 128 (0.01 mg/mL) formulation. After 4 hours, nanoparticles were aspirated and 150 µL of 0.05% trypsin was used for detachment of cells from wells. After incubation for 15 minutes, 300 µL FACS buffer was used to neutralise the trypsin and cells were centrifuged at 1500 rpm for 10 minutes. Following this, cells were stained with Zombie Violet (1:500) dye for 30 minutes at room temperature in order to help with gating on live cells. Then, cells were fixed with 100 µL of 4% paraformaldehyde in PBS for 20 minutes. Fixed cells were centrifuged, and pellets resuspended in 50 µL of PBS. Data were acquired using an Image Stream 100 (Amnis, Seattle, US) and on single cell in focus events was used for analysis. Ideas Software (Amnis, Seattle, WA, USA) was used for data analysis. Total cell fluorescence was calculated by default total cell masks for the measurement of the nanoparticle internalisation and cell interiors were identified using the area erode tool (brightfield channel). Internalisation index was shown as percentage of maximum internalisation (percentage of interior cell fluorescence to total cell fluorescence).

In Vitro Bone marrow dendritic cell (BM DC) Transfection Experiments

C57BL/6 female mice were purchased from Charlie River UK. *In vivo* Femurs and tibias were collected from 6-12 week old C57BL/6 female mice and bone marrow cells were released by mortar and pestle in complete RPMI media. Red blood cells were lysed with ACK lysis buffer and washed with complete media. Remaining progenitor cells were plated 2x10^6 cells/ml in a 24 well non-tissue culture treated plate with 150ng/ml Flt3-L. On day 8, BM DCs were transfected with the polyplexes at 1 µg/mL mRNA and 128 µg/mL PBAE concentrations and left for 24 h incubation. On day 9, cells were harvested and labelled for surface staining as detailed in supplementary table 1. Flow cytometer data was collected on a Fortessa instrument and analysed via FlowJo software Version 10.

Statistical analysis

Graphs and statistics were prepared in GraphPad Prism 9.5.1 version or higher. Statistical differences were analysed using either one-way or two-way ANOVA adjusted for multiple comparison (either Tukey's or Dunnet's), p value lower than 0.05 was considered as statically significant and the levels of statistical significance were set $p^* < 0.05$, $p^{**} < 0.01$, $p^{***} < 0.001$ and $p^{****} < 0.0001$.

Results and discussion

Synthesis and Characterisation of PBAEs

A synthetic pathway consisting of four steps was employed to synthesise the targeted poly(beta amino ester) (PBAE), modified covalently with TLR7 agonist Loxoribine, (Figure 2A). For the first step, 1,4-butanediol diacrylate (BDD) was reacted with 5-aminopentanol (5AP) using a molar excess of BDD to yield a PBAE terminated with acrylic groups, pBDD-5AP. This PBAE was chosen due to previous preclinical studies showing high mRNA transfection capability both *in vitro* and *in vivo* [37]. The successful synthesis of the acrylic terminated PBAE, pBDD-5AP was confirmed using ^{1}H NMR spectroscopy, as signals around 6.3 - 5.9 ppm on the ^{1}H NMR spectrum indicated the presence of double bonds (Spectrum S1). p(BDD-5AP) was then end-capped with 2,2'-

View Article Online
DOI: 10.1039/D5BM01812A

(ethylenodioxy)bis(ethylamine) via a further aza-Michael addition to yield the amine terminated PBAE H_2N-(pBDD-5AP)-NH_2 which was confirmed as the ^1H NMR spectrum indicated complete a disappearance of acrylic end-groups (Spectrum S2). H_2N-(pBDD-5AP)-NH_2 was further transformed with N-hydroxysuccinimidyl- 3-mercaptopropanoate to yield the thiol end-capped PBAE HS-(p(BDD-5AP)-SH polymer. The success of this modification was proved by the appearance of two signals characteristic to 3-mercaptopropionate group - at 2.90 ppm coming from alpha-methylene group to the thiol moiety and 2.20 ppm coming from the thiol group (Spectrum S3). The thiol groups were then used as a reactive handle to conjugate Loxoribine to the PBAEs, which contain a double bond making it suitable for thiol-ene chemistry under UV irradiation leading to the final product LOX-p(BDD-5AP)-LOX. Due to difficulties with analysis of an NMR spectrum of the final product, as a small molecule was conjugated with the polymer, Figure 2the successful conjugation with Loxoribine was demonstrated using HPLC and UV-Vis spectroscopy experiments (see Supplementary Information Figure S3). These methodologies allowed determination of the total content of Loxoribine in the final polymer, which was found to be approximately 27 µg per mg PBAE (w/w 2.7%). All intermediate products and the final product were characterised by means of GPC (Figure 2B and 2C) where the molar mass was observed to increase after each end modification step (6200, 6600, 6900 and 7800 g mol^{-1}) and monomodal chromatograms with around $Đ$ =1.4 were revealed. The buffering capacities were assessed for H_2N-(pBDD-5AP)-NH_2 and LOX-(pBDD-5AP)-LOX as the pKa of polycations has been recognised as crucial for enhancing endosomal buffering and endo/lysosomal escape of polymer-based nucleic acid delivery systems (Figure 2D). Acid-base titration in the pH range of 10.0-3.0 for amine-end-capped PBAE titration curve was observed between the negative control (NaCl) and positive control (PEI). However, with LOX-end-capped PBAE the titration curve was similar to that of PEI, indicating that LOX-end-capping increased their buffering capacity (Figure 2D), likely due to the purine rings of LOX even though only 2 drug molecules were added to each polymer chain.

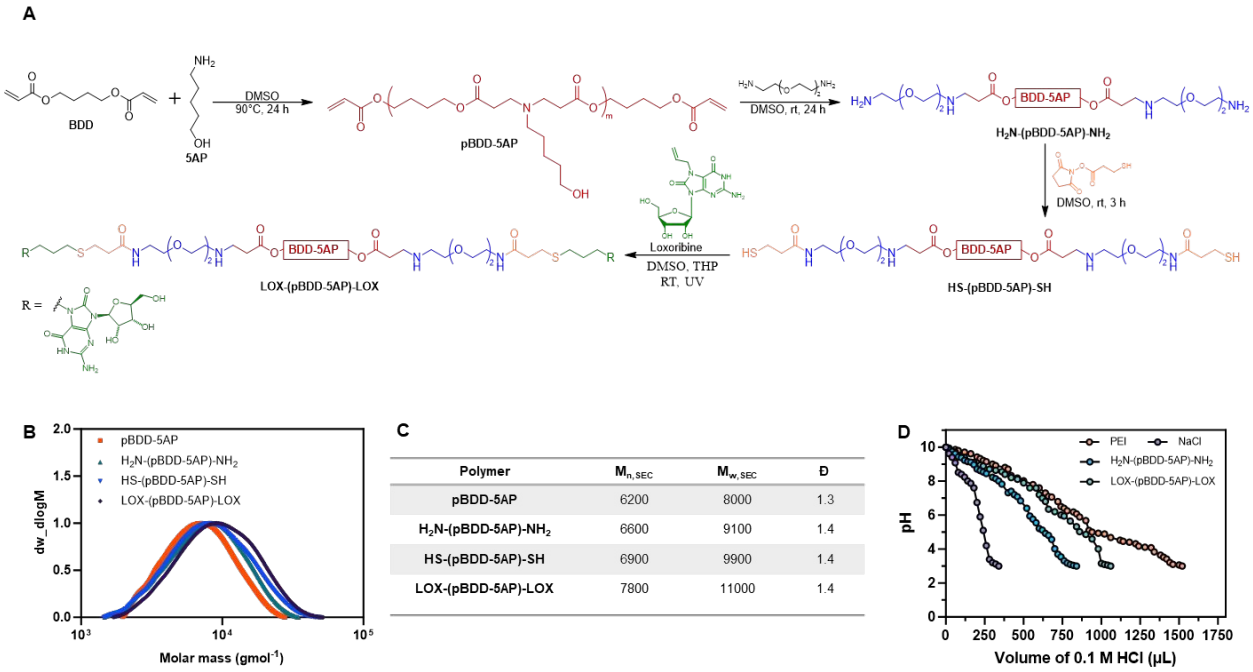

Figure 2. Synthesis and characterisation of PBAEs. *(A)* Synthetic scheme for step-growth Michael-addition polymerisation of BDD, 5-AP then end-capped utilizing 2,2'-(Ethylenedioxy)bis(ethylamine) and 3-Mercaptopropanyl-N-hydroxysuccinimide ester to produce LOX-end-capped PBAE (Step 4). *(B)* Molecular weights of PBAEs determined using GPC and *(C)* the molecular weight distribution of pBDD-5AP, H_2N-(pBDD-5AP)-NH2, SH-(pBDD-5AP)-SH and LOX-(pBDD-5AP)-LOX. (D) Buffering capacity of H2N-(pBDD-5AP)-NH2 and LOX-(pBDD-5AP)-LOX compared to polyethyleneimine (PEI) and negative control of a 0.1 M NaCl(aq) solution.

View Article Online
DOI: 10.1039/D5BM01812A

Polyplex Physicochemical Properties of different end-capped polyplexes

Polyplex preparation was performed at three different polymer / fluc saRNA weight-to-weight ratios (w/w ratios of 32, 64 and 128) for H_2N-(pBDD-5AP)-NH_2 and LOX-(pBDD-5AP)-LOX PBAEs. Solutions of saRNA and the polymers were prepared using 25 mM NaOAc buffer then the nucleic acid solution was dropwise added to polymer solution as 1:1 volume ratio using pipette. The prepared nanoparticles were incubated at room temperature for 30 minutes prior to use. Experiments were then performed to define physicochemical and biological characteristics of the polyplexes, encompassing particle size, surface charge, encapsulation efficiency, biocompatibility, and RNA expression (see Figure 3A).

Hydrodynamic diameters of all nanoparticles were observed to be between 100-200 nm with low polydispersity index (PDI) values (< 0.2) determined by dynamic light scattering (DLS) (Figure 3B), with no major changes in particle size observable across different w/w ratios. Notably, LOX-(pBDD-5AP)-LOX polyplexes were larger than the H_2N-(pBDD-5AP)-NH_2 polyplexes, suggesting that end modification of the polymer with LOX affected the structures of the polyplexes. We reasoned that this could be due to the removal of the free NH_2 end groups to the more bulky but possibly less protonated (at ambient pH) purine groups of LOX which changed the sterics and electrostatics of the complexation interactions with RNA. However, the hydrodynamic diameters of LOX-(pBDD-5AP)-LOX polyplexes were significantly decreased with increasing w/w ratios possibly due to the increased cation content that can induce more compact structures, consistent with previous reports on polyplexes [38].

Next, the zeta potentials of the particles were measured using DLS. Notably, higher zeta potential values were revealed for LOX-(pBDD-5AP)-LOX polyplexes (24 ± 8 mV) compared to H_2N-(pBDD-5AP)-NH_2 (20 ± 2 mV), which could be due to the LOX addition, as mentioned -above due to the purine rings of LOX and increased surface-exposed charges on the polyplexes (Figure 3C). The encapsulation efficiency of nanoparticles was analysed utilizing a Ribogreen assay and showed full RNA encapsulation for all nanoparticles produced at all ratios (Figure 3D). Finally, TEM micrographs of all polyplexes prepared at a w/w ratio of 128 indicated mostly spherical complexes between 25 to 280 nm in diameter consistent with DLS analysis, and allowing for some particle shrinking during dehydration for TEM (Figure 3E). Furthermore, as DLS analysis can over represent larger particles present in heterogeneous particle distributions, it is likely that any smaller species visible by TEM may not have been included in the particle size averages [39]. TEM images are intended for qualitative visualisation; apparent aggregation may result from negative staining and may not fully reflect the native nanoparticle structure. Overall, these results indicate that all six polyplexes were capable of encapsulating saRNA and producing particle sizes below the typical 200 nm diameter threshold for efficient gene delivery.

View Article Online
DOI: 10.1039/D5BM01812A

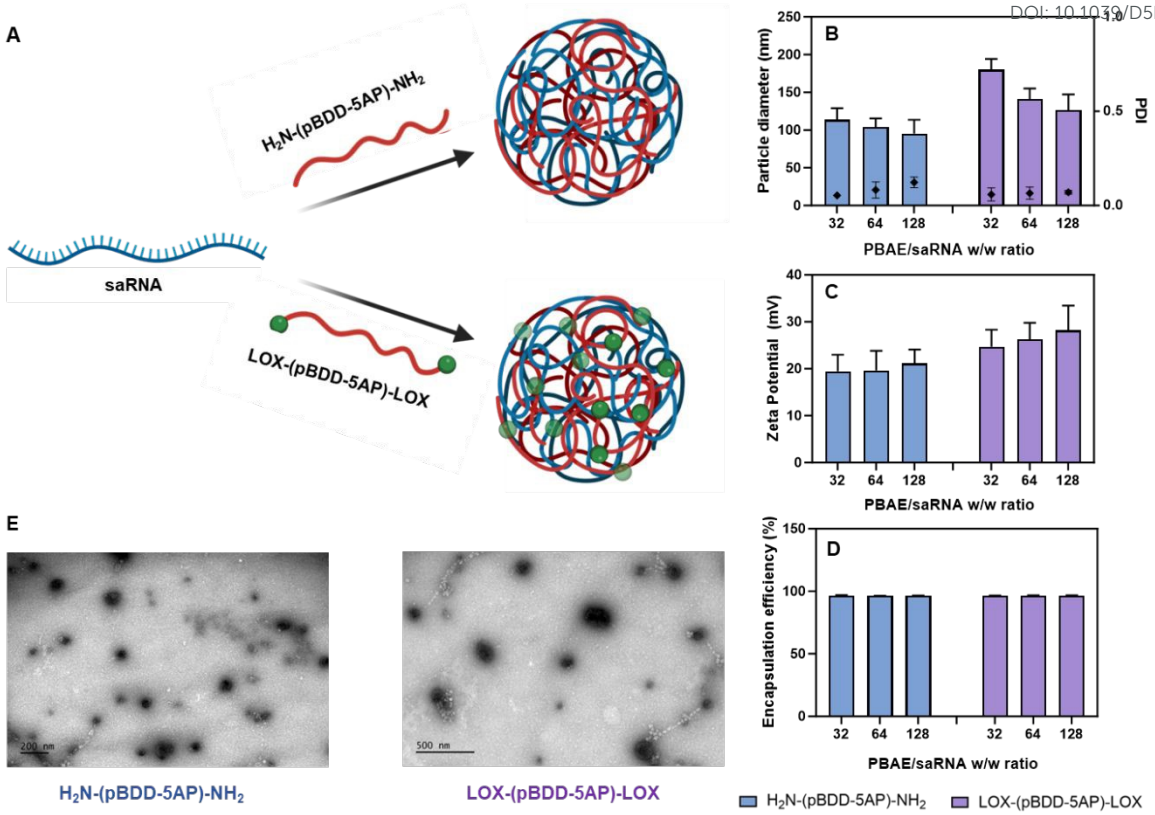

Figure 3. Formulation of PBAEs with saRNA to produce polyplex nanoparticles. (*A*) Schematic representation of saRNA formulation with H_2N-(pBDD-5AP)-NH_2 and LOX-(pBDD-5AP)-LOX prepared in 25 mM sodium acetate pH 5.0 at a final saRNA concentration of 10 µg/mL. (*B*) Particle size and (*C*) zeta potential for the H_2N-(pBDD-5AP)-NH_2 and LOX-(pBDD-5AP)-LOX polyplexes at a PBAE/saRNA w/w ratio of 32, 64 and 128 determined by dynamic light scattering at 25˚C. Bars represent the mean ± SD. (*D*) Encapsulation efficiency of saRNA within polyplexes evaluated using Ribogreen assay. Bars represent the mean ± SD. (*E*) Representative transmission electron micrograph of the polyplexes H_2N-(pBDD-5AP)-NH_2 and LOX-(pBDD-5AP)-LOX. All data are presented as mean ± SD, with n = 3 for all conditions. Statistical significance was determined using a two-way ANOVA test, with $P < 0.05$ considered significant.

In Vitro Evaluation of RNA Delivery

Transfection and metabolic activity of different end-capped polyplexes

The acute toxicity and saRNA delivery efficiency of individual formulations H_2N-(pBDD-5AP)-NH_2 and LOX-(pBDD-5AP)-LOX were evaluated in HEK293T cells (as a model cell line) and DC2.4 cells (a relevant dendritic cell line for vaccines). Similar to the formulation characterisation study described earlier, polyplexes were prepared at polymer/saRNA w/w ratios of 32, 64, and 128 using firefly luciferase encoding saRNA. These were compared against lipofectamine (as the positive expression control) and Triton X-100 (as the positive toxicity control).

All formulations demonstrated higher viability values (over 80% as inferred from metabolic activity) compared to positive control Lipofectamine (50%) (Figure 4A and 4B). It can be implied that the conjugation of Loxoribine did not affect the metabolic activity in these cell lines. Similar to previous studies, increasing w/w ratios of H_2N-(pBDD-5AP)-NH_2 resulted in increased toxicity due to increased polycation concentration which is known to disrupt the negative phospholipid bilayer [40, 41] (Figure 4A). Interestingly, there was no substantial difference detected for LOX-(pBDD-5AP)-LOX formulations despite the increasing w/w ratios. In terms of transfection efficiency, in general, saRNA expression was slightly lower for the LOX-(pBDD-5AP)-LOX formulations compared to amine end-capped analogues (Figure 4C and 4D). This could be due to the above-mentioned slightly bigger nanoparticle diameters of the LOX-end-capped formulations where the cellar uptake could be lower. Notably, increasing w/w ratios of the formulations in both cell lines resulted in higher transfection [42]. In HEK293T cells, the transfection efficiencies of w/w ratio 128 were lower than Lipofectamine; however, in CD2.4 cells, both formulations (w/w 128) showed as high transfection efficiency as positive control.

View Article Online
DOI: 10.1039/D5BM01812A

Given the lower transfection efficiencies of the Loxoribine conjugated PBAE in both HEK293Ts and DC2.4s, we wanted to evaluate if co-incubation of free Loxoribine caused the same effect. To decouple the effect of Loxoribine from polymer end-group modification, cells were treated with amine-end-capped PBAE/saRNA polyplexes (w/w 128) in the presence of increasing concentrations of free Loxoribine (0–100 μg/mL), covering the LOX-equivalent range present in LOX-(pBDD-5AP)-LOX formulations, and compared to naked saRNA controls (Figure 4E and 4F). Loxoribine addition at all concentrations did not meaningfully influence transfection efficiency in both HEK293Ts and DC2.4s. This contrasts with other studies which when an mRNA delivery system is co-formulated with a TLR agonist, the expression of the delivered mRNA reduces by several orders of magnitude due to the downstream expression of pro-inflammatory cytokines inhibiting the cells ribosomal protein synthesis machinery [43]. This effect seems to be TLR dependent with TLR3 activation exhibiting the most potent reduction in RNA expression, while TLR7 and TLR9 have a moderate effect and minimal effect respectively. Given that once stimulated, most TLR pathways lead to the same pro-inflammatory pathways, this TLR dependent mechanism may instead be due to the non-selective activation of other PRRs by specific adjuvants, such as polyI:C which not only antagonises TLR3 but also cytosolic RNA sensors. In our case, the minimal effect on transfection efficiency when spiked with free Loxoribine, especially in DC2.4's which are known to express TLR7, was an encouraging indication that adjuvancy with Loxoribine should not compromise protein expression [31].

View Article Online
DOI: 10.1039/D5BM01812A

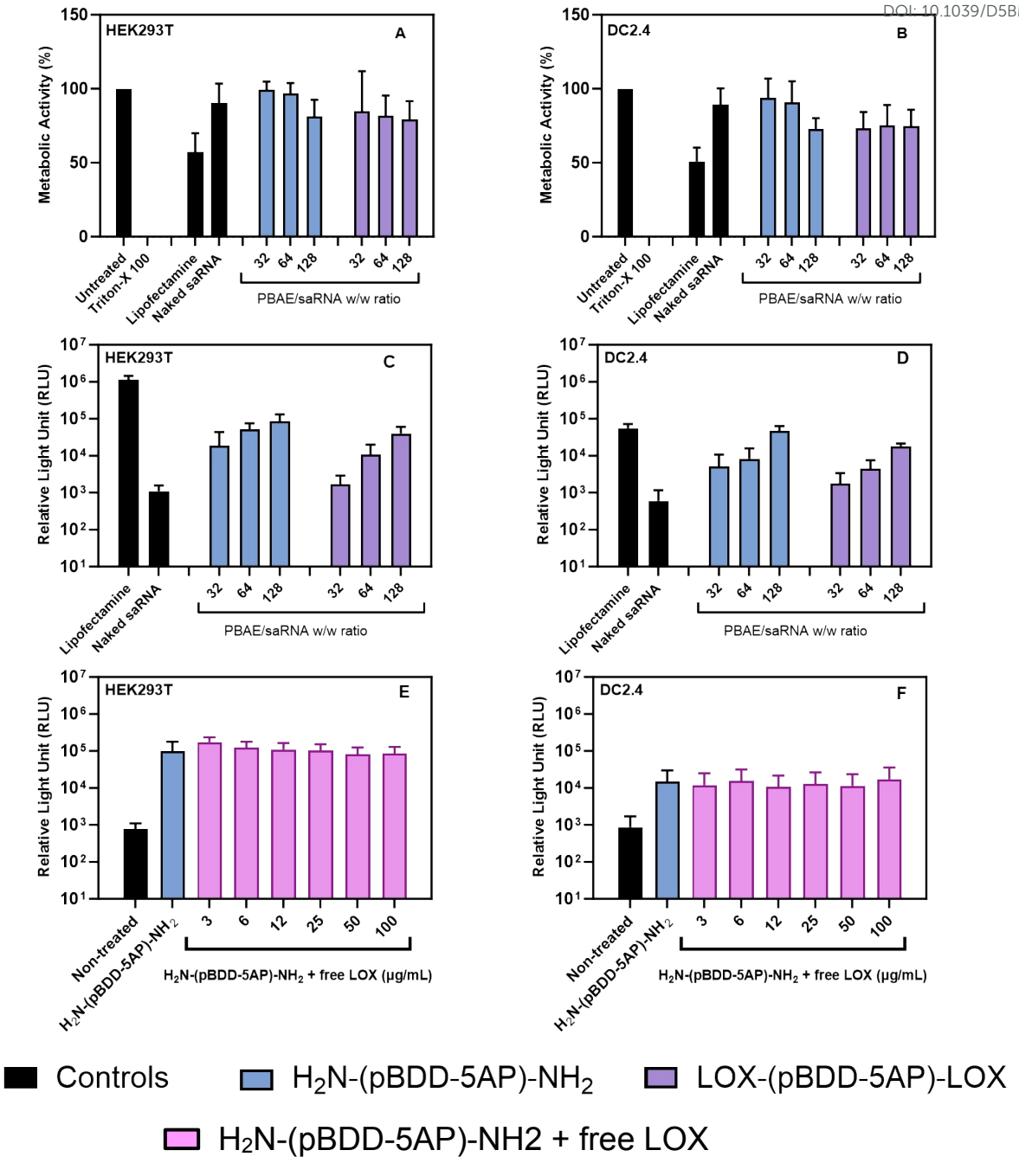

Figure 4. Metabolic activity and transfection efficiency of PBAE derived saRNA polyplexes. Effect of PBAE polyplexes formulated with firefly luciferase encoding saRNA at PBAE/saRNA w/w ratios of 32, 64 and 128 on metabolic activity (*A* and *B*) and transfection efficiency (*C* and *D*) on HEK293T cells (*A* and *C*) and DC2.4 cells (*B* and *D*). Cells were treated with polyplexes containing saRNA at a concentration of 500 ng/mL (100 ng/well) in serum-free Opti-MEM. Metabolic activity was compared against Triton X (positive control) and untreated cells (negative control), and calculated by normalizing metabolic activity to untreated cells. In vitro transfection efficiency was analysed after 24 h post-transfection using the Promega ONE-GLO luciferase assay and compared against Lipofectamine Messenger MAX™ (positive control) and naked saRNA (negative control) expressed as relative light units (RLU) for luciferase expression. *(E-F)* RLU for H_2N-(pBDD-5AP)-NH_2 and H_2N-(pBDD-5AP)-NH_2 + free LOX dilutions (3-100 µg/mL) in HEK293T and DC2.4 cells. Bars represent the mean ± SD. All data are presented as mean ± SD, with n = 3 for all conditions. Statistical significance was determined using a two-way ANOVA test, with $P < 0.05$ considered significant.

View Article Online
DOI: 10.1039/D5BM01812A

TLR7 Activation Assay

Having observed high transfection efficiencies from the Loxoribine conjugated PBAEs in both HEK293T and DC2.4 cell lines, we then evaluated the Loxoribine conjugated PBAEs, LOX-(pBDD-5AP)-LOX and its counterpart polyplexes to stimulate intracellular TLR7 compared against free Loxoribine. This was achieved by using an engineered HEK cell line, HEK-Blue™ TLR7, which has been transduced to co-express TLR7 with an NF-kB-inducible secreted embryonic alkaline phosphatase (SEAP) reporter gene which can be detected by the conversion of the SEAP-induced hydrolysis of its corresponding substrate into a UV (650 nm) absorbing product (Figure 5A). Similar to the formulation characterisation studies described earlier, polyplexes were prepared at PBAE/saRNA w/w ratios of 32, 64, and 128 using firefly luciferase encoding saRNA. Using the data from our quantification assays to determine Loxoribine conjugation, we compared the polyplexes produced to the equivalent concentrations of non-formulated LOX-(pBDD-5AP)-LOX to examine the potential synergy when complexed with saRNA, which itself can stimulate TLR7, and against free Loxoribine to determine the effect of conjugation (Figure S4D). These were assessed against lipofectamine (as the positive expression control) and Triton X-100 (as the positive toxicity control). High metabolic activity values (> 90%) were demonstrated for all treatments with no major decrease in viability for all free Loxoribine, LOX-(pBDD-5AP)-LOX and saRNA polyplex concentrations in accordance with the non-transgenic HEK293T cells tested above and therefore would not impact the expression of SEAP to assess TLR7 activation (Figure S4A and S4C and 5C).

Because Loxoribine is covalently conjugated to the polymer backbone, its effective intracellular dose is governed by nanoparticle uptake and endosomal trafficking rather than extracellular concentration. As such, classical dose response analyses used for free small-molecule agonists are not directly translatable to this system. Instead, we compared free and conjugated Loxoribine at matched LOX-equivalent concentrations to assess functional preservation and enhancement of TLR7 signalling.

Quantification with the SEAP reporter revealed a dose dependent increase in $OD_{650\ nm}$ with increasing free Loxoribine concentrations (Figure S4B). Both free H_2N-(pBDD-5AP)-NH_2 and the resulting polyplex exhibited lower or a statistically insignificant different in OD_{650} compared to the equivalent concentrations of free Loxoribine due to the absence of Loxoribine or weak activation of TLR7 alone by saRNA when encapsulated. Free LOX-(pBDD-5AP)-LOX exhibited a dose-dependent increase in TLR7 activation, with free polymer concentrations at the equivalent of polyplex at w/w 128 exhibiting 50% higher $OD_{650\ nm}$ than the corresponding concentration of free Loxoribine (25 µg/mL). This indicated that conjugation of LOX to the polymer enhances its TLR7 antagonisation effect (Figure 5B). This may be due to enhanced uptake of Loxoribine, or enhanced trafficking to the endosome where the receptor resides due to an increase in apparent size when conjugated. In addition, the LOX-(pBDD-5AP)-LOX polyplexes at w/w 128 exhibited the highest $OD_{650\ nm}$ of 0.55; this was over 2-fold higher than the equivalent concentration of free Loxoribine and was likely caused by the combination of saRNA and Loxoribine. From these results it is reasonable to suggest that TLR7 activation of conventional mRNA polyplexes can be boosted by the addition of a TLR7 agonist, which also exhibits an increase in activity from being transported to the endosome in either nanoparticle or polymer form. Interestingly, lipofectamine delivered saRNA did not exhibit any statistically significant TLR7 activation over the untreated control, which may suggest a difference between lipid and polymer delivery systems (Figure 5B).

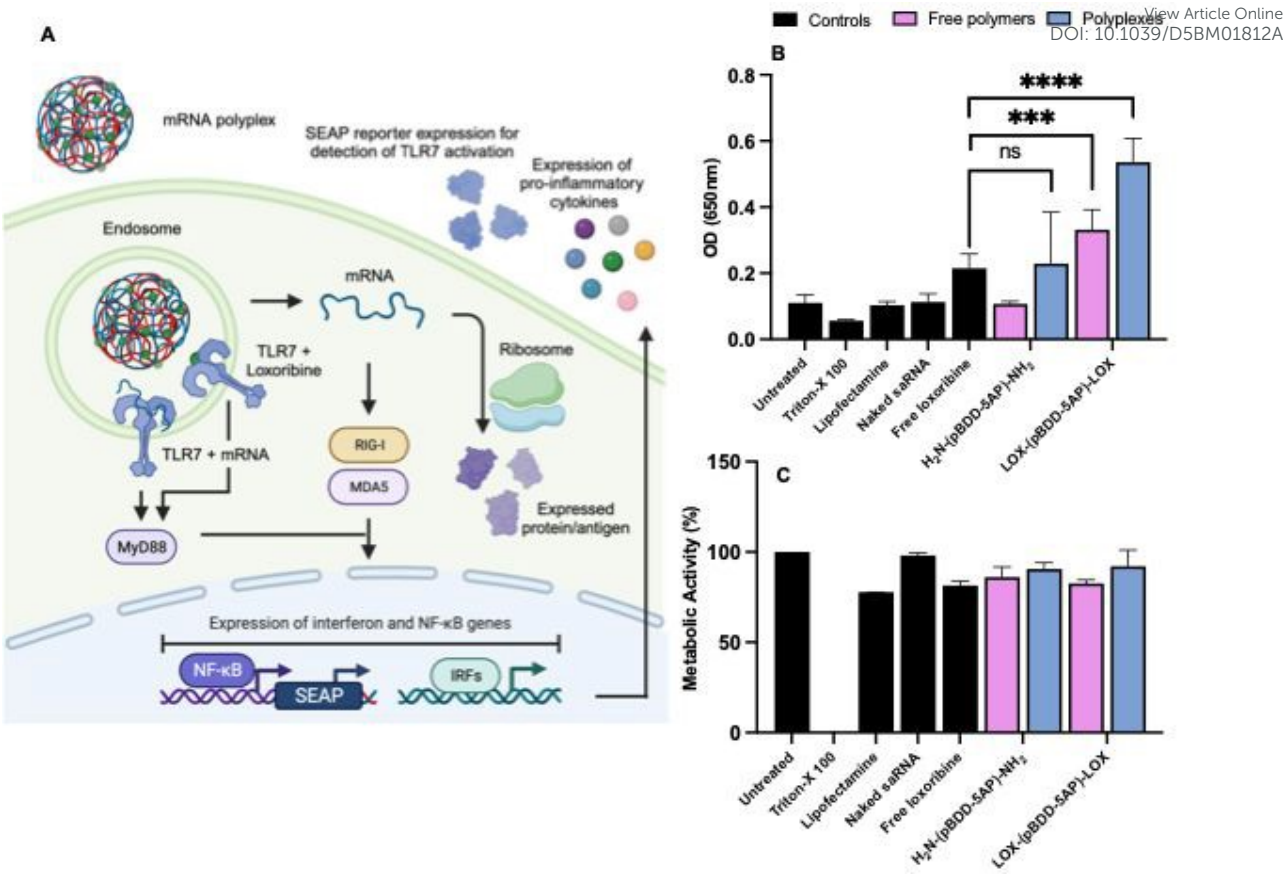

Figure 5. TLR7 Activation Assay using HEK-BLUE cells. *(A)* Schematic representation of nanoparticle uptake and TLR7 activation. *(B)* The determination of the TLR7 activation capacity of amine and **L**oxoribine-end-capped polymers and nanoparticles (w/w 128) compared to controls in HEK-BLUE cells. The concentration of free lox was 25 µg/mL *(C)* Metabolic activity of the amine and **L**oxoribine-end-capped polymers and nanoparticles (w/w 128) compared to controls in HEK-BLUE cells. All data are presented as mean ± SD, with n = 3 for all conditions. Statistical significance was determined using a two-way ANOVA test, with $P < 0.05$ considered significant ($p^{***} < 0.001$ and $p^{****} < 0.0001$).

Cellular uptake of polyplexes

Due to the encouraging transfection, toxicity and TLR7 receptor activation profiles of LOX-(pBDD-5AP)-LOX polyplex at w/w 128, we investigated further the extent of internalisation of these polyplexes. Therefore, we first generated a FITC labelled LOX-(pBDD-5AP)-LOX through isothiocyanate reaction at the pendant hydroxyl groups of the 5-AP monomers within the core PBAE. Imaging flow cytometry was utilised to evaluate the cellular uptake of selected polyplex as 2 h and 4 h after treatment (Figure 6A to 6C). The successful cell association of the nanoparticles using DC2.4 cells was evaluated through FITC intensity, and the histogram of the 2 h and 4 h indicates the increased intensity of FITC fluorescence observed (Figure 6B). The median fluorescence intensity value at 2 h incubation was around 60000, and expectedly, the intensity further increased to around 80000 at 4 h incubation time. High internalisation can explain the high transfection efficiencies of the LOX-(pBDD-5AP)-LOX w/w 128 polyplexes. In addition to cellular uptake scores, the internalisation vs membrane association of nanoparticles for each cell can be analysed using imaging flow cytometry. In this study, the median of internalisation score of the polyplexes was approximately 1.7 indicating a high proportion of nanoparticles were internalised inside the cells since having a score less than 0.3 can be considered to be surface bound (Figure S3) [44].

In order to assess further the intracellular internalisation mechanism of the selected nanoparticle LOX-(pBDD-5AP)-LOX w/w 128 in HEK293T and DC2.4 cells, we employed confocal microscopy to evaluate colocalization with a lysosomal (Lysotracker™ red) and nuclear (Hoecht 33342) stain (Figure 6D). After

View Article Online
DOI: 10.1039/D5BM01812A

2 h post administration, confocal micrographs showed that polyplexes successfully internalised within the cells and merged images demonstrated with minimal co-localisation with the acidic lysosomes. This was analysed with imageJ indicating Pearson's Correlation Coefficient between FITC labelled polyplexes and Lysotracker™ stained lysosomes were below 0.5 (0.3 for HEK293T and 0.4 for DC2.4 cells). Slightly higher co-localisation values were detected for DC2.4 (0.4) cells compared to HEK293T cells (0.3), which may be one of the reasons of low transfection of dendritic cells. Since, given the ~200 nm particle diameters it is likely that these formulations were internalised by an endocytosis mechanism, however the apparent low colocalization with the acidic lysosomes may indicate that the particles escaped before endosomal maturation to lysosomal compartments. This successful endosomal escape could also be due to TLR7 activation as this is where the TLR7 receptor is and where it would be activated with LOX-conjugated carriers. Although further endosomal escape studies are required to investigate this phenomenon in more detail, it is possible that enhanced endosomal escape was a factor in the high expression efficiencies observed for these complexes.

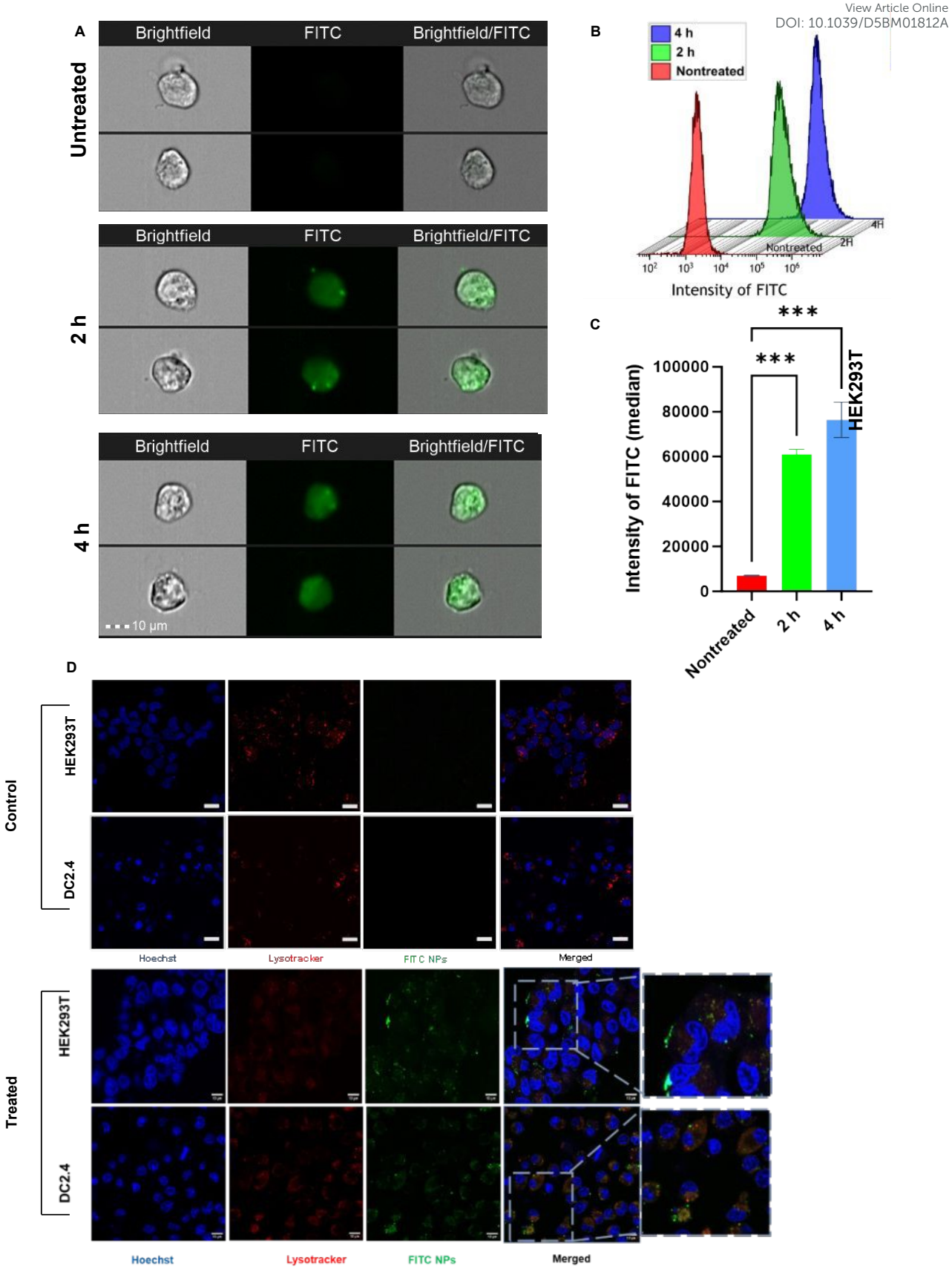

Figure 6. Cellular uptake of PBAE derived saRNA polyplexes. (*A*) Imaging flow cytometry images for DC2.4 cells after 2 h and 4 h following treatment with FITC-labelled LOX-(pBDD-5AP)-LOX polyplexes at a PBAE/saRNA w/w ratio 128 at 500 ng/well (500 ng/mL) (Scale bar 10 µm) *(B)* histograms of fluorescence intensity and *(C)* median fluorescence values Data were analysed using IDEAS software and Kaluza. *(D)* Representative live cell confocal microscopy images of HEK293T and DC2.4 cells for both Control (Untreated) and Treated groups 2 h post-

View Article Online
DOI: 10.1039/D5BM01812A

transfection with a firefly luciferase encoding saRNA formulated with LOX-(pBDD-5AP)-LOX at a PBAE/saRNA w/w ratio of 128 at 100 ng/well (500 ng/mL) saRNA. Scale bar 10 μm (63x). Representative control (untreated) live-cell confocal microscopy images of HEK293T and DC2.4 cells in Figure S4.

Transfection and activation of bone marrow derived dendritic cells

To further investigate the ability of our Loxoribine conjugated PBAEs and derived polyplexes to activate conventional Dendritic Cells (cDCs), we determined transfection and activation of primary murine bone marrow-derived cDCs (BMDCs). Given the wide body of evidence indicating that m1ψ containing mRNA reduces the intrinsic stimulation of TLRs and other PRRs [45, 46], for these experiments we opted to formulate polyplexes using eGFP encoding mRNA instead of saRNA. Polyplexes derived from LOX-(pBDD-5AP)-LOX and H_2N-(pBDD-5AP)-NH_2 were formulated at a polymer/mRNA w/w ratio of 128, which exhibited the highest expression in DC2.4s (Figure 4D). These were then incubated with BMDCs at 1 μg/mL mRNA for 24 h and compared against LOX-(pBDD-5AP)-LOX and H_2N-(pBDD-5AP)-NH_2 as free polymers, free Loxoribine as a positive control and fresh media as an untreated control. Cells were analysed by flow cytometry for expression of eGFP as a marker for transfection efficiency and CD86 and MHC II indicators of DC activation. (Figure 6A).

View Article Online
DOI: 10.1039/D5BM01812A

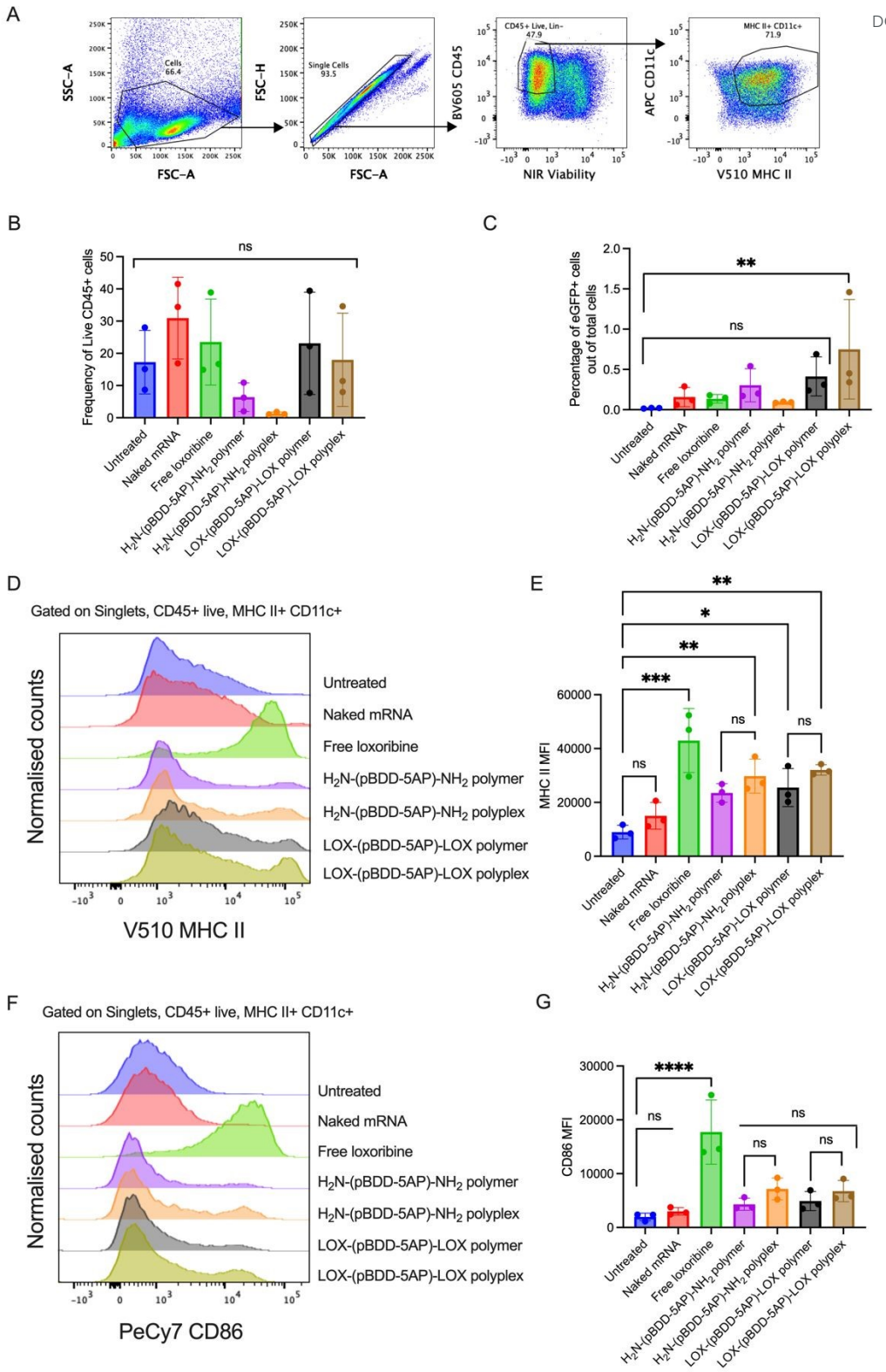

Figure 7. BMDC transfection efficiency and activation markers after treatment with H_2N-(pBDD-5AP)-NH_2 or LOX-(pBDD-5AP)-LOX free polymers and their polyplex formulations at 1 µg/mL mRNA at a mRNA/polymer w/w ratio of 128. (*A*) Representative gating strategy of BM DCs. Cells were gated on singlets, live CD45+, Lin- (Linage includes CD19, B220, CD3, Ly6c, Ly6G and CD64 to gate out monocytes, neutrophils, macrophages, plasmacytoid DCs, CD4 T cells and CD8 T cells) MHC II+ CD11c+ cells. (*B*) Bar graph showing the frequency of Live CD45+ of live singlets of the different conditions. (*C*) Bar graph showing the percentage of eGFP+ cells out of total live CD45+ cells. (*D*). Representative histogram of MHC II expression of the BM DCs gated as shown in (A). (*E*). Bar graph showing the MHC II Mean Fluorescence Intensity (MFI) of each condition. (*F*) Representative histogram of CD86 expression of the BM DCs gated as shown in (A). (*G*) Bar graph showing the CD86 (MFI) of each condition. All

View Article Online
DOI: 10.1039/D5BM01812A

data are presented as mean ± SD, with n = 3 for all conditions. Statistical significance was determined using a one-way ANOVA test, with $P < 0.05$ considered significant.

We observed that there was no statistically significant change in cell viability across the formulations, however there was relatively large variability across the three replicates due to each replicate culture being derived from individual mice (Figure 6B). Only the LOX-(pBDD-5AP)-LOX polyplex condition displayed statistically significant eGFP expression over the untreated control, exhibiting a modest 1% eGFP+ cells of the total cells collected (Figure 6C). Free Loxoribine, the positive control, increased MHCII expression in majority of the BM DCs. We observed an increase in MHCII expression with the polyplexes compared to the untreated control. However, there was no clear difference in MHC II expression between the control polymers (without Loxoribine conjugation) compared to the Loxoribine conjugated PBAEs, suggesting the polymers themselves may be intrinsically activating these pathways (Figure 6D and 6E). There was a small increase in cells producing high levels of MHC II in the LOX-(pBDD-5AP)-LOX polyplex condition, which is indicative of strong activation (Figure 6D).

A similar expression pattern is seen for CD86, with free Loxoribine inducing high levels of CD86 with the polyplexes. With no significant difference between of MHC II between the polyplexes and polymers (Fig 6F-6G). In contrast to findings observed from the HEK-BLUE TLR7 assay (Figure 5) which showed that our Loxoribine conjugated exhibited higher stimulation of the TLR7 receptor, the Loxoribine conjugated PBAEs and derived polyplexes did not exhibit higher CD86 expression or MHCII than free Loxoribine in the BMDC model (Figure 6D-6G). This may be due to a difference in uptake of the polymers in BMDCs relative to the HEK-Blue cells.

Conclusion

In conclusion, the development of messenger RNA technology has accelerated the translation of innovative vaccines and treatments. The search for safe and effective delivery systems for RNA medicines has led to a focus on nanoparticle-based carriers, particularly the promising avenue of polycations such as PBAEs. Despite challenges related to immune activation and translation efficiency, recent advances have been made towards improving these delivery systems. This study introduces a new and potentially important advance - a TLR7a-conjugated polycation using Loxoribine for self-amplifying mRNA formulations. Through the synthetic pathway and formulation process, these polymers successfully encapsulated the cargo, resulting in small polyplex nanoparticles with notable transfection efficiency and minimal cytotoxicity. Importantly, the TLR7 activation assays demonstrated the significant potential of LOX-end-capped formulations to induce TLR7 signalling, surpassing amine-end-capped PBAE-based formulations and Lipofectamine. These findings highlight the promise of LOX-end-capped formulations at w/w ratio 128 for not only enhancing mRNA delivery but also activating crucial immune pathways. Conjugating Loxoribine directly to the polymer, rather than formulating it into an LNP, avoids the uncertainty around its positioning and retention, which is typically challenging with conventional cationic lipid-based systems. While this work employed photo-initiated thiol-ene chemistry due to its simplicity and accessibility, we acknowledge that alternative bioorthogonal chemistries, such as tetrazine-thiol exchange with subsequent alkene locking, may offer advantages in terms of selectivity and characterisation. Incorporating such strategies represents a valuable direction for future optimization of these delivery systems.

Acknowledgements

We thank the Royal Society [Wolfson Research Merit Award WM150086 to CA]. Work on this project is supported by Wellcome Leap as part of the R3 Program [Biofoundry-in-a-Box] and Turkish Ministry of National Education. CG/CB were supported by a PhD studentship from the Percy Stevens Foundation. We also thank Esme Ireson and Paul Cooling for expert technical support. The Nanoscale & Macroscale Research Centre (NMRC) is acknowledged for providing the facilities for TEM and related analysis

particularly to Denise McLean. We thank the School of Life Sciences imaging facility (SLIM) and their staff, particularly Dr Tim Self, for use of their facilities and expert guidance.

View Article Online
DOI: 10.1039/D5BM01812A

Author contributions

Conceptualization, H.B., C.A. and P.G.; data curation and formal analysis, H.B., A.E., R.J.K., C.G., N.G., C.L.B., C.A. and P.G. writing original draft preparation, H. B.; writing review and editing, H.B., A.E., R.J.K., C.G., N.G., C.L.B., C.A. and P.G.; supervision, C.A. and P.G.; project administration, C.A.; funding acquisition, H.B. and C.A. All authors have read and agreed to the published version of the manuscript.

Conflict of Interest

All authors declare that they have no conflicts of interest.

Data access statement

All relevant data can be obtained upon request from the corresponding authors at p.gurnani@ucl.ac.uk and cameron.alexander@nottingham.ac.uk

View Article Online
DOI: 10.1039/D5BM01812A

References

[1] M. Chehelgerdi, M. Chehelgerdi, The use of RNA-based treatments in the field of cancer immunotherapy, Molecular Cancer 22(1) (2023) 106.
[2] L. Miao, Y. Zhang, L. Huang, mRNA vaccine for cancer immunotherapy, Molecular Cancer 20(1) (2021) 1-23.
[3] N. Pardi, M.J. Hogan, F.W. Porter, D. Weissman, mRNA vaccines—a new era in vaccinology, Nature reviews Drug discovery 17(4) (2018) 261-279.
[4] M. Karam, G. Daoud, mRNA vaccines: Past, present, future, Asian journal of pharmaceutical sciences (2022).
[5] Z.A. Azrak, M.S. Taha, J. Jagal, A. Elsherbeny, H. Bayraktutan, M.H. AbouGhaly, A.H. Elshafeey, K. Greish, M. Haider, Optimized mucoadhesive niosomal carriers for intranasal delivery of carvedilol: A quality by design approach, International Journal of Pharmaceutics (2024) 123935.
[6] N.K. Dastgerdi, N.K. Dastgerdi, H. Bayraktutan, G. Costabile, F. Atyabi, R. Dinarvand, G. Longobardi, C. Alexander, C. Conte, Enhancing siRNA cancer therapy: Multifaceted strategies with lipid and polymer-based carrier systems, International Journal of Pharmaceutics (2024) 124545.
[7] A. Akinc, M.A. Maier, M. Manoharan, K. Fitzgerald, M. Jayaraman, S. Barros, S. Ansell, X. Du, M.J. Hope, T.D. Madden, The Onpattro story and the clinical translation of nanomedicines containing nucleic acid-based drugs, Nature nanotechnology 14(12) (2019) 1084-1087.
[8] P. Gurnani, A.K. Blakney, J. Yeow, C.R. Bouton, R.J. Shattock, M.M. Stevens, C. Alexander, An improved synthesis of poly (amidoamine) s for complexation with self-amplifying RNA and effective transfection, Polymer Chemistry 11(36) (2020) 5861-5869.
[9] B. Fayed, J. Jagal, R. Cagliani, R.A. Kedia, A. Elsherbeny, H. Bayraktutan, G. Khoder, M. Haider, Co-administration of amoxicillin-loaded chitosan nanoparticles and inulin: A novel strategy for mitigating antibiotic resistance and preserving microbiota balance in Helicobacter pylori treatment, International Journal of Biological Macromolecules 253 (2023) 126706.
[10] H. Bayraktutan, P. Symonds, V.A. Brentville, C. Moloney, C. Galley, C.L. Bennett, A. Mata, L. Durrant, C. Alexander, P. Gurnani, Sparsely PEGylated poly (beta-amino ester) polyplexes enhance antigen specific T-cell response of a bivalent SARS-CoV-2 DNA vaccine, Biomaterials (2024) 122647.
[11] P. Gurnani, A.K. Blakney, R. Terracciano, J.E. Petch, A.J. Blok, C.R. Bouton, P.F. McKay, R.J. Shattock, C. Alexander, The in vitro, ex vivo, and in vivo effect of polymer hydrophobicity on charge-reversible vectors for self-amplifying RNA, Biomacromolecules 21(8) (2020) 3242-3253.
[12] C. Fornaguera, J.F. Alarcon, A. Masoero, I. Pagnotta, R. Vaya, P. Castells-Colldeforns, M. Losada, M. Guarro, M. Lecina, G. Sitia, Polymeric nanoparticle-loaded extracellular vesicles as biomimetic nucleic acid vaccines, (2025).
[13] K.M. Steinegger, L. Allmendinger, S. Sturm, F. Sieber-Schäfer, A.P. Kromer, K. Müller-Caspary, B. Winkeljann, O.M. Merkel, Molecular dynamics simulations elucidate the molecular organization of poly (beta-amino ester) based polyplexes for siRNA delivery, Nano Letters 24(49) (2024) 15683-15692.
[14] H. Bayraktutan, R. Kopiasz, A. Elsherbeny, P. Gurnani, C. Alexander, Poly (beta-amino esters): applications in immunology, Chemical Science (2026).
[15] N. Puigmal, V. Ramos, N. Artzi, S. Borrós, Poly (β-amino ester) s-based delivery systems for targeted transdermal vaccination, Pharmaceutics 15(4) (2023) 1262.
[16] M. Navalón-López, A. Dols-Perez, S. Grijalvo, C. Fornaguera, S. Borrós, Unravelling the role of individual components in pBAE/polynucleotide polyplexes in the synthesis of tailored carriers for specific applications: on the road to rational formulations, Nanoscale advances 5(6) (2023) 1611-1623.
[17] N. Qiao, M. Hori, M. Naito, H. Chang, S. Ogura, M. Suzuki, T. Kimura, S. Fukushima, H.J. Kim, S. Uchida, Increasing polycation hydrophobicity in mRNA polyplex vaccines enhances the efficacy of humoral and cellular immunity induction, Biomaterials 324 (2026) 123515.

[18] P. Dosta, A.M. Cryer, M.Z. Dion, T. Shiraishi, S.P. Langston, D. Lok, J. Wang, S. Harrison, T. Hatten, M.L. Ganno, Investigation of the enhanced antitumour potency of STING agonist after conjugation to polymer nanoparticles, Nature nanotechnology 18(11) (2023) 1351-1363.
[19] U. Sahin, K. Karikó, Ö. Türeci, mRNA-based therapeutics—developing a new class of drugs, Nature reviews Drug discovery 13(10) (2014) 759-780.
[20] F. Heil, P. Ahmad-Nejad, H. Hemmi, H. Hochrein, F. Ampenberger, T. Gellert, H. Dietrich, G. Lipford, K. Takeda, S. Akira, The Toll-like receptor 7 (TLR7)-specific stimulus loxoribine uncovers a strong relationship within the TLR7, 8 and 9 subfamily, European journal of immunology 33(11) (2003) 2987-2997.
[21] V. Gote, P.K. Bolla, N. Kommineni, A. Butreddy, P.K. Nukala, S.S. Palakurthi, W. Khan, A comprehensive Review of mRNA vaccines, International journal of molecular sciences 24(3) (2023) 2700.
[22] S. Qin, X. Tang, Y. Chen, K. Chen, N. Fan, W. Xiao, Q. Zheng, G. Li, Y. Teng, M. Wu, mRNA-based therapeutics: powerful and versatile tools to combat diseases, Signal transduction and targeted therapy 7(1) (2022) 166.
[23] A. Elsherbeny, H. Bayraktutan, U.C. Oz, C. Moloney, J.C. Ashworth, A.M. Grabowska, C. Alexander, Responsive Nanomaterial Delivery Systems for Pancreatic Cancer Management, Advanced Therapeutics (2023) 2300330.
[24] A. Kowalczyk, F. Doener, K. Zanzinger, J. Noth, P. Baumhof, M. Fotin-Mleczek, R. Heidenreich, Self-adjuvanted mRNA vaccines induce local innate immune responses that lead to a potent and boostable adaptive immunity, Vaccine 34(33) (2016) 3882-3893.
[25] A.A. Smith, E.C. Gale, G.A. Roth, C.L. Maikawa, S. Correa, A.C. Yu, E.A. Appel, Nanoparticles Presenting Potent TLR7/8 Agonists Enhance Anti-PD-L1 Immunotherapy in Cancer Treatment, Biomacromolecules 21(9) (2020) 3704-3712.
[26] M. Luchner, S. Reinke, A. Milicic, TLR agonists as vaccine adjuvants targeting cancer and infectious diseases, Pharmaceutics 13(2) (2021) 142.
[27] D.N. Toussi, P. Massari, Immune adjuvant effect of molecularly-defined toll-like receptor ligands, Vaccines 2(2) (2014) 323-353.
[28] N. Chaudhary, L.N. Kasiewicz, A.N. Newby, M.L. Arral, S.S. Yerneni, J.R. Melamed, S.T. LoPresti, K.C. Fein, D.M. Strelkova Petersen, S. Kumar, Amine headgroups in ionizable lipids drive immune responses to lipid nanoparticles by binding to the receptors TLR4 and CD1d, Nature Biomedical Engineering 8(11) (2024) 1483-1498.
[29] A.E. Zelkoski, Z. Lu, G. Sukumar, C. Dalgard, H. Said, M.-G. Alameh, E. Mitre, A.M. Malloy, Ionizable lipid nanoparticles of mRNA vaccines elicit NF-κB and IRF responses through toll-like receptor 4, npj Vaccines 10(1) (2025) 73.
[30] S. Abbasi, S. Uchida, Multifunctional immunoadjuvants for use in minimalist nucleic acid vaccines, Pharmaceutics 13(5) (2021) 644.
[31] A.K. Blakney, P.F. McKay, C.R. Bouton, K. Hu, K. Samnuan, R.J. Shattock, Innate inhibiting proteins enhance expression and immunogenicity of self-amplifying RNA, Molecular Therapy 29(3) (2021) 1174-1185.
[32] B. Wilson, K.M. Geetha, Lipid nanoparticles in the development of mRNA vaccines for COVID-19, Journal of Drug Delivery Science and Technology 74 (2022) 103553.
[33] A.M. Weiss, S. Hossainy, S.J. Rowan, J.A. Hubbell, A.P. Esser-Kahn, Immunostimulatory polymers as adjuvants, immunotherapies, and delivery systems, Macromolecules 55(16) (2022) 6913-6937.
[34] J. Huete-Carrasco, R.I. Lynch, R.W. Ward, E.C. Lavelle, Rational design of polymer-based particulate vaccine adjuvants, European Journal of Immunology (2023) 2350512.
[35] H. Bayraktutan, R.J. Kopiasz, A. Elsherbeny, M.M. Espuga, N. Gumus, U.C. Oz, K. Polra, P.F. McKay, R.J. Shattock, P. Ordóñez-Morán, Polysarcosine functionalised cationic polyesters efficiently deliver self-amplifying mRNA, Polymer Chemistry 15(18) (2024) 1862-1876.
[36] N.K. Dastgerdi, N. Gumus, H. Bayraktutan, D. Jackson, K. Polra, P.F. McKay, F. Atyabi, R. Dinarvand, R.J. Shattock, L. Martinez-Pomares, Charge neutralized poly (β-amino ester) polyplex nanoparticles for delivery of self-amplifying RNA, Nanoscale Advances (2024).

[37] G.T. Zugates, N.C. Tedford, A. Zumbuehl, S. Jhunjhunwala, C.S. Kang, L.G. Griffith, D.A. Lauffenburger, R. Langer, D.G. Anderson, Gene delivery properties of end-modified poly (β-amino ester) s, Bioconjugate chemistry 18(6) (2007) 1887-1896.
[38] N.M. Hamelmann, S. Uijttewaal, S.D. Hujaya, J.M. Paulusse, Enhancing Cellular Internalization of Single-Chain Polymer Nanoparticles via Polyplex Formation, Biomacromolecules 23(12) (2022) 5036-5042.
[39] S.K. Filippov, R. Khusnutdinov, A. Murmiliuk, W. Inam, L.Y. Zakharova, H. Zhang, V.V. Khutoryanskiy, Dynamic light scattering and transmission electron microscopy in drug delivery: a roadmap for correct characterization of nanoparticles and interpretation of results, Materials Horizons 10(12) (2023) 5354-5370.
[40] C.H. Jones, M. Chen, A. Ravikrishnan, R. Reddinger, G. Zhang, A.P. Hakansson, B.A. Pfeifer, Mannosylated poly (beta-amino esters) for targeted antigen presenting cell immune modulation, Biomaterials 37 (2015) 333-344.
[41] Z. Zhang, K. Wen, C. Zhang, F. Laroche, Z. Wang, Q. Zhou, Z. Liu, J.P. Abrahams, X. Zhou, Extracellular nanovesicle enhanced gene transfection using polyethyleneimine in HEK293T cells and zebrafish embryos, Frontiers in bioengineering and biotechnology 8 (2020) 448.
[42] I. González-Domínguez, E. Puente-Massaguer, J. Lavado-García, L. Cervera, F. Gòdia, Micrometric DNA/PEI polyplexes correlate with higher transient gene expression yields in HEK 293 cells, New Biotechnology 68 (2022) 87-96.
[43] E. Ben-Akiva, J. Karlsson, S. Hemmati, H. Yu, S.Y. Tzeng, D.M. Pardoll, J.J. Green, Biodegradable lipophilic polymeric mRNA nanoparticles for ligand-free targeting of splenic dendritic cells for cancer vaccination, Proceedings of the National Academy of Sciences 120(26) (2023) e2301606120.
[44] Y. Phanse, A.E. Ramer-Tait, S.L. Friend, B. Carrillo-Conde, P. Lueth, C.J. Oster, G.J. Phillips, B. Narasimhan, M.J. Wannemuehler, B.H. Bellaire, Analyzing cellular internalization of nanoparticles and bacteria by multi-spectral imaging flow cytometry, JoVE (Journal of Visualized Experiments) (64) (2012) e3884.
[45] T.E. Mulroney, T. Pöyry, J.C. Yam-Puc, M. Rust, R.F. Harvey, L. Kalmar, E. Horner, L. Booth, A.P. Ferreira, M. Stoneley, N 1-methylpseudouridylation of mRNA causes+ 1 ribosomal frameshifting, Nature 625(7993) (2024) 189-194.
[46] K. Karikó, H. Muramatsu, F.A. Welsh, J. Ludwig, H. Kato, S. Akira, D. Weissman, Incorporation of pseudouridine into mRNA yields superior nonimmunogenic vector with increased translational capacity and biological stability, Molecular therapy 16(11) (2008) 1833-1840.

View Article Online
DOI: 10.1039/D5BM01812A

Data access statement

All relevant data can be obtained upon request from the corresponding authors at p.gurnani@ucl.ac.uk and cameron.alexander@nottingham.ac.uk